Hindawi
Shock and Vibration
Volume 2021, Article ID 7236077, 11 pages
https://doi.org/10.1155/2021/7236077

Research Article

Numerical Simulation of Cracking Failure and Weakening Law of Roadway Surrounding Rock under High Stress

Feng Cheng, Ai-jun Chen, Di Wu, Xian-yuan Tang, and Chun-hui Su

School of Architecture and Transportation Engineering, Guilin University of Electronic Technology, Guilin 541004, China

Correspondence should be addressed to Ai-jun Chen; caj3026@163.com

Received 2 August 2021; Accepted 20 September 2021; Published 28 October 2021

Academic Editor: Fan Deyuan

In deep roadway mining, high water pressure causes rock mass cracking and weakens the overall strength, affecting the stability of underground metal mine mining roadways. Therefore, using a numerical simulation method, we analyzed the strain softening characteristics of rocks after the inflexion point of elasticity and studied the strain distribution and the minimum support resistance under high-pressure groundwater conditions. Considering the groundwater pressure and effective porosity on the strain softening characteristics of the surrounding rocks, we investigated the critical groundwater pressure under which the surrounding rocks would remain stable. Actual engineering verification helps to obtain the supporting characteristic curves under different influencing factors. We found that water pressure and effective porosity are the significant factors that decide the development scope of the plastic zone. The more significant the increase of the plastic zone, the more notable the changes in the support curve. Moreover, the plastic zone is likely to occur when the hydraulic head is between 30 and 50 m; when the hydraulic head exceeds 50 m, it is likely to produce a relaxation zone.

1. Introduction

The stress behavior caused by groundwater pressure in roadway excavation of nonferrous metal mines is a major factor affecting the stability of surrounding rocks. The surrounding rocks of roadways excavated under high water pressure show obvious softening characteristics and reduced strength [1, 2]. Because the surrounding rock of excavated roadways is subject to long-term physical and chemical reactions caused by pore water, its effective stress, rock stiffness, and stability usually decrease when it remains saturated with water [3, 4]. Sun et al. carried out triaxial tests under water-saturated conditions to study carbonaceous shale [5]. They found that the compressive strength of rocks changed as the confining pressure changed. Under low confining pressures, the compressive strength of rocks was affected by the time they saturated with water. Besides, the attenuation curve shows an exponential distribution. However, under high confining pressures, the compressive strength of rocks was not affected by the time they saturated with water [6, 7].

Huang et al. obtained the permeability change law and cracking mechanism of deep rock mass under hydraulic pressure through experimental research on the permeability of deep roadway floor rock mass. Huang et al. used the true triaxial experimental system to study the influence of hydraulic fracture propagation and proposed a system of controlled fracture methods such as directional hydraulic slitting and fracturing [8, 9]. Zhu et al. studied the mechanism of rock instability in mining roadway by establishing the model and obtained the law of the change after the stress disturbance of surrounding rock [2, 10, 11]. Jiang et al. analyzed the process of rock burst caused by the breakdown force of high water pressure by studying groundwater's accumulation effect in the mining process of deep roadway. They put forward the corresponding prevention and control measures [12–14]. However, they did not analyze the stress-strain relationship caused by rock burst [15]. Most published studies have researched the elastic-plastic deformation of surrounding rocks in excavated roadways under water-rich conditions by combining theoretical research with numerical calculations. However, since these studies do not

consider the effect of strength attenuation after the peak strength of surrounding rocks is reached, the results cannot be applied to actual experiments. Most softening constitutive models of surrounding rocks are linear softening models. The effect of groundwater seepage, especially the effect of high groundwater pressure, is often neglected in structural stress analyses of the surrounding rock mass. Since the water depth of high water pressure mining roadways is generally more than 30 m, and its initial ground stress is relatively low [16, 17]; it is necessary to consider the mechanical characteristics of nonlinear strain softening of surrounding rocks in order to truly reflect the stress-strain relationship of deep surrounding rocks. This is especially necessary for elucidating the stress-strain relationship of locally fractured rocks or soft rocks under high water pressure. Therefore, based on the nonlinear softening model of surrounding rocks [18], the present study analyzed the elastic-plastic zone of surrounding rocks in deeply excavated roadways, discussed the various parameters that would influence the mechanical characteristics of surrounding rocks, and determined a relatively accurate law for displacement and stress distribution of the elastic-plastic zone of surrounding rocks, considering the seepage of high-pressure groundwater and different drainage conditions of the mining roadway.

2. Theoretical Analysis of the Fracture Failure of Surrounding Rock Mass

2.1. Analysis of Initial Strain Characteristics of Surrounding Rock Mass. The constitutive relationship of the surrounding rock mass is in accordance with the stress-strain relationship of rocks under uniaxial compression. The constitutive model established by Zhao (2019) has general applicability to rocks [19–21], which can accurately reflect the relationship between peak intensity and strain. The model is described as follows:

$$\begin{cases} \sigma = E\varepsilon, & when\ \varepsilon \le \varepsilon_c, \\ \sigma = \sigma_c \dfrac{\varepsilon/\varepsilon_c}{g\left(\varepsilon/\varepsilon_c - 1\right)^2 + \varepsilon/\varepsilon_c}, & \text{when } \varepsilon > \varepsilon_c, \end{cases} \tag{1}$$

where E is the elastic modulus; σ_c is the peak strength expressed as $\sigma_c = 2c\cos\phi/(1-\sin\phi)$, in which c is the cohesion of the rock and φ is the angle of internal friction; g is a test parameter and $g = 7.264 \times 10^{-4}{\sigma_c}^2$; the value of g differs before and after the peak strength, which is applicable to all rocks, and 0.25 is taken as the inflexion point for the value of g. ε_c is the peak strain, expressed as $\varepsilon_c = (1300 + 10\sigma_c) \times 10^{-6}$.

In order to test and verify the stress-strain changes and strain softening characteristics of rocks after the peak strength, this study analyzes the test results of four types of rocks as in Table 1.

When $\varphi = 30^\circ$ (average), 4 MPa, 5 MPa, 6 MPa, and 7 MPa are taken as values of σ_c to illustrate the relationship between σ_c and ε; the relationship curves are shown in Figure 1.

According to Figure 1, the stresses and strains of the four rocks show strain softening characteristics after reaching the peak strength. After reaching the peak strength, the stress decreases and the strain increases. The results show that the model has universal applicability to describing the strain softening characteristics of rocks after the peak strength is reached. When this model is applied to actual engineering problems, however, it is necessary to carry out fitting analyses with real rock test data to obtain the actual expressions for g and ε_c.

2.2. Basic Assumptions for Mechanical Calculation.

(1) It is assumed that the section of the excavated roadway is circular. The area includes an elastic zone and a plastic zone. The radius of the roadway is set as a, the calculated radius of the plastic zone is R, and the calculated radius of the elastic zone is b. The calculation model is shown in Figure 2.

(2) To facilitate calculation, it is assumed that the rock strata above the calculated area of the roadway are not subject to any influence from mining, and the thickness of the overlying strata is $h = b - a$.

(3) It is assumed that the surrounding rock is homogeneous and isotropic and has μ as its Poisson's ratio, φ as its effective porosity, the ratio of the volume of interconnected pores in the rock to the total volume of the rock, the characteristics of porous media, and a lateral pressure coefficient of 1 ($\lambda = 1$). The gravity stress is σ_b, pore water pressure is p_f, groundwater pressure is p_0, and roadway support force is p_a at the center of the roadway.

(4) Because the roadway is axisymmetric and subject to uniform pressure, $\sigma_1 = \sigma_\theta$ and $\sigma_3 = \sigma_r$. If the excavated roadway is infinitely long, the strain problem can be treated as a plane problem, that is, $\varepsilon_z = \varepsilon_2 = 0$.

(5) It is assumed that groundwater seepage has a stable flow and follows Darcy's law of seepage and hydraulic movement principles [22, 23].

(6) It is assumed that the calculation parameters do not change with the groundwater environment after rock burst, and the calculation parameters are invariants in the calculation process [24–26].

3. Analysis of Nonlinear Weakening Model of Surrounding Rock

3.1. Distribution Law of Pore Water Pressure in Elastic-Plastic Zone of Surrounding Rock. Affected by highly enriched groundwater, there is a pressure difference between the inside and the outside of the roadway, forming an elastic zone and a plastic zone. In addition, the groundwater will flow along the stratum fissures and cause seepage [27, 28]. It is assumed that the seepage has stable flow and thus follows Darcy's law of seepage. According to the hydraulic movement principles of groundwater in rock strata, the pore water

Table 1: Rock test results.

Sample no.	Poisson's ratio μ	Elasticity modulus E (GPa)	Gravity γ (kN · m^{-3})	Cohesionc (MPa)	Pore water pressure coefficient φ (°)
1	0.312	24.84	21.95	0.371	31
2	0.353	25.61	23.72	0.352	29
3	0.347	23.43	22.43	0.347	34
4	0.371	25.77	23.66	0.418	32

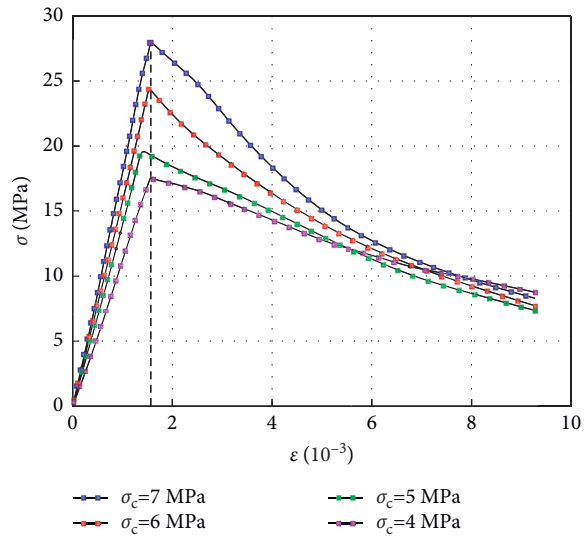

Figure 1: Relationship between σ and ε during rock softening.

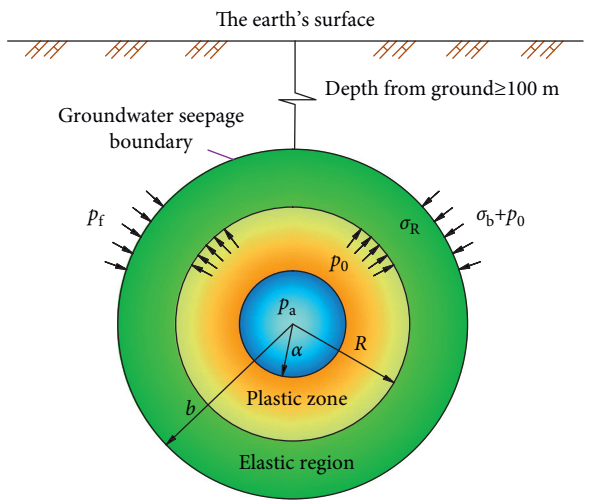

Figure 2: Mechanical calculation model.

pressure in the elastic-plastic zone presents the following distribution law [29].

(1) In the plastic zone, $a \le r \le R$, and thus

$$p = p_1 + (p_R - p_1)\frac{\ln(r/a)}{\ln(R/a)}, \tag{2}$$

where p_1 is the pore water pressure on the wall of the roadway and p_R represents the pore water pressure in the plastic zone.

(2) The flow velocity $r = R$, which satisfies the condition of continuous interstitial flow:

$$p_R = \frac{p_f \ln(R/a) + p_1 \rho \ln(b/R)}{\ln(R/a) + \rho \ln(b/R)}, \tag{3}$$

where ρ is the coefficient ratio, $\rho = K_p/K_e$, K_p is the permeability coefficient of surrounding rocks in the plastic zone, and K_e is permeability coefficient of surrounding rocks in the elastic zone.

3.2. Analysis of Stress and Displacement of Surrounding Rock in Elastic Zone. According to the mechanical equilibrium equation (30), the stress of the surrounding rock mass satisfies the following relation:

$$\frac{d\sigma_r}{dr} + \frac{\sigma_r - \sigma_\theta}{r} + \phi\frac{dp}{dr} = 0, \tag{4}$$

where ϕ is the pore water pressure coefficient.

By deriving (4) and combining it with (2), the following equation is obtained:

$$\frac{dp}{dr} = \frac{p_f - p_R}{r\ln(b/R)}. \tag{5}$$

Combining the plane physical equation and the axisymmetric geometric equation [19], it can be found that $\varepsilon_r = d\overline{u}/dr$, $\varepsilon_\theta = \overline{u}/r$, and $\gamma_{r\theta} = 0$. The displacement equilibrium equation is described as follows:

$$\frac{d^2\overline{u}}{dr^2}+\frac{1}{r}\frac{d\overline{u}}{dr}-\frac{\overline{u}}{r^2}=\frac{F_1\nu}{rE}, \tag{6}$$

where $F_1=\phi p_f-p_R/\ln(R/b)$, $\nu=(1+\mu)(1-2\mu)/(1+\mu)$, μ is the volume compression coefficient, and $\overline{u}$ is the radial displacement.

By solving (6), the expression for the radial displacement $\overline{u}$ is obtained:

$$\overline{u}=C_1r+\frac{C_2}{r}+\frac{F_1\nu}{2E}r \quad \ln r \tag{7}$$

where the two parameters C_1 and C_2 are integral constants.

The above integral constants, C_1 and C_2, can be determined by the displacement boundary conditions in the elastic zone, that is, $\sigma_r|r=b=\sigma_b+p_0$ and $\sigma_r|r=R=\sigma_R$. The expression of stress distribution can be obtained as follows:

$$\sigma_r^e=\sigma_b+p_0+\frac{F_1}{2}(1+\nu_1) \quad \ln\frac{r}{b}+\frac{R^2}{R^2-b^2}\left(\frac{b^2}{r^2}-1\right)\left[\sigma_b+p_0-\sigma_R+\frac{F_1}{2}(1+\nu_1)\ln\frac{R}{b}\right], \tag{8}$$

$$\sigma_\theta^e=\sigma_b+p_0+\frac{F_1}{2}\left[(1+\nu_1)\ln\frac{r}{b}+(\nu_1-1)\right]-\frac{R^2}{R^2-b^2}\left(\frac{b^2}{r^2}+1\right)\left[\sigma_b+p_0-\sigma_R+\frac{F_1}{2}(1+\nu_1)\ln\frac{R}{b}\right], \tag{9}$$

where $\nu_1=\mu/1-\mu$, and σ_R is the radial stress (at the interface between elastic and plastic zones).

The displacement calculated by using (9) is expressed as the absolute displacement. However, before the roadway is excavated, there is a certain initial displacement in the surrounding rock, and this initial displacement should be deducted in calculations for practical scenarios. Thus, the relative radial displacement after deduction is expressed as

$$\overline{u}=C_1r+\frac{C_2}{r}+\frac{F_1\nu}{2E}r \quad \ln r-\frac{r(1+\mu)(1-2\mu)}{E}(\sigma_b+p_0). \tag{10}$$

3.3. Analysis of Stress and Displacement of Surrounding Rock in Plastic Zone. In the plastic zone of surrounding rocks in mining roadways, the rock has different degrees of compressive deformation. To facilitate displacement analysis, it is assumed that the volume is incompressible in the plastic zone. Therefore,

$$\varepsilon_r+\varepsilon_\theta+\varepsilon_z=0, \tag{11}$$

$$\begin{aligned}\overline{u}&=A/r,\\ \varepsilon_\theta&=A/r^2,\\ \varepsilon_r&=-A/r^2.\end{aligned} \tag{12}$$

where A is an integral constant.

According to the assumption made in Section 2.2, when the mining roadway is infinitely long ($\varepsilon_z=0$), the equivalent effect $\varepsilon_i$in the plastic zone is replaced by (12), and thus,

$$\varepsilon_i=\frac{\sqrt{2}}{3}\sqrt{(\varepsilon_r-\varepsilon_\theta)^2+(\varepsilon_z-\varepsilon_r)^2+(\varepsilon_z-\varepsilon_\theta)^2}=\frac{2}{\sqrt{3}}\frac{A}{r^2}. \tag{13}$$

When $r=R$, $\varepsilon_i=\varepsilon_c$, thus,

$$A=\frac{\sqrt{3}}{2}R^2\varepsilon_c. \tag{14}$$

The displacement in (12) and the equivalent strain in (14) are integrated into .

$$\begin{aligned}\overline{u}&=\frac{\sqrt{3}}{2}\frac{R^2\varepsilon_c}{r},\\ \varepsilon_i&=\varepsilon_c\frac{R^2}{r^2}.\end{aligned} \tag{15}$$

Since the volume is incompressible in the plastic zone, $\sigma_z^p=1/2(\sigma_r^p+\sigma_\theta^p)$, and the equivalent stress can be expressed as follows:

$$\begin{aligned}\sigma_i&=\frac{1}{\sqrt{2}}\sqrt{(\sigma_r^p-\sigma_\theta^p)+(\sigma_z^p-\sigma_r^p)+(\sigma_z^p-\sigma_\theta^p)}\\ &=\frac{1}{\sqrt{2}}\sqrt{(\sigma_\theta^p+\sigma_r^p)}.\end{aligned} \tag{16}$$

It is assumed that the ultimate bearing capacity occurs in the complex stress state, and it is not unloaded during the loading process. Consequently, the proportional relationship of the stress components varies with the loading. Therefore, the traditional constitutive equation of the plastic stage, i.e., (1), can be generalized and applied by using Henck's total strain theory in plastic mechanics [30, 31]. The relationship between the equivalent stress and equivalent strain of the rock mass under complex stress states can be obtained as follows:

$$\sigma_i=\sigma_c\frac{\varepsilon_i/\varepsilon_c}{g(\varepsilon_i/\varepsilon_c-1)^2+\varepsilon_i/\varepsilon_c}. \tag{17}$$

In addition, under the condition of seepage, the equivalent stress follows the equilibrium equation [32, 33], which satisfies the equilibrium equation expressed in

$$\frac{d\sigma_r^p}{dr}+\frac{\sigma_r^p-\sigma_\theta^p}{r}+\phi\frac{dp}{dr}=0. \tag{18}$$

By substituting (15) and (16) into (18), and combining the result with (17), the following equation is obtained:

$$\sigma_r^p = \begin{cases} \dfrac{2\sigma_c}{\sqrt{3}\sqrt{4g-1}} \arctan\left(\dfrac{2gr^2/R^2-(2g-1)}{\sqrt{4g-1}}\right) + F_2 \ln r + C, & \text{when } g > 0.25, \\ -\dfrac{\sigma_c}{\sqrt{3}\sqrt{4g-1}} \ln\left|\dfrac{2gr^2/R^2-(2g-1)+\sqrt{1-4g}}{2gr^2/R^2-(2g-1)-\sqrt{1-4g}}\right| + F_2 \ln r + C, & \text{when } g < 0.25, \end{cases} \tag{19}$$

where $F_2 = \phi p_R - p_1/\mathrm{In}\,(a/R)$, and C is an integral constant. According to the model established by [34, 35], the value g takes 0.25 as the inflexion point: the value exceeds 0.25 before the strength peak, and it is lower than 0.25 after the peak.

According to the boundary conditions of the plastic zone, that is, $\sigma_r^p|_{r=a} = p_a$, the radial stress of the plastic zone is obtained as follows:

$$\sigma_r^p = \begin{cases} p_a + \dfrac{2\sigma_c}{\sqrt{3}\sqrt{4g-1}}\left(\arctan\dfrac{2gr^2/R^2-(2g-1)}{\sqrt{4g-1}} - \arctan\dfrac{2ga^2/R^2-(2g-1)}{\sqrt{4g-1}}\right) + F_2 \ln\dfrac{r}{a}, & \text{when } g > 0.25, \\ p_a + \dfrac{\sigma_c}{\sqrt{3}\sqrt{1-4g}}\left(\ln\left|\dfrac{2ga^2/R^2-(2g-1)+\sqrt{1-4g}}{2ga^2/R^2-(2g-1)-\sqrt{1-4g}}\right| - \ln\left|\dfrac{2gr^2/R^2-(2g-1)+\sqrt{1-4g}}{2gr^2/R^2-(2g-1)-\sqrt{1-4g}}\right|\right) + F_2 \ln\dfrac{r}{a}, & \text{when } g < 0.25. \end{cases} \tag{20}$$

In the same way, the relation between σ_θ^p and σ_r^p in (16) can be obtained as follows:

$$\begin{aligned} \sigma_\theta^p &= 2{\sigma_i}^2 - \sigma_r^p \\ &= \frac{2\sigma_c}{\sqrt{3}} \frac{R^2/r^2}{g\left(R^2/r^2-1\right)^2 + R^2/r^2} - \sigma_r^p. \end{aligned} \tag{21}$$

3.4. Determination of Radius R of Plastic Zone. When $r = R$, the mining roadway is symmetrical, and therefore the stress in the elastic zone of surrounding rocks on the other side of the roadway is also in accordance with (16). Thus, (22) is obtained.

$$\sigma_R^e = \sigma_b + p_0 + \frac{F_1}{2}(1+\nu_1) \ln\frac{R}{b} - \frac{b^2-R^2}{2b^2}\left[\frac{2\sigma_c}{\sqrt{3}} - \frac{F_1}{2}(\nu_1 - 1)\right]. \tag{22}$$

The stress in the plastic zone of the surrounding rocks on the other side of the mining roadway can be obtained by using (19), that is,

$$\sigma_R^p = \begin{cases} p_a + \dfrac{2\sigma_c}{\sqrt{3}\sqrt{4g-1}}\left(\arctan\dfrac{1}{\sqrt{4g-1}} - \arctan\dfrac{2ga^2/R^2-(2g-1)}{\sqrt{4g-1}}\right) + F_2 \ln\dfrac{r}{a}, & \textit{when } g > 0.25; \\ p_a + \dfrac{\sigma_c}{\sqrt{3}\sqrt{1-4g}}\left(\ln\left|\dfrac{2ga^2/R^2-(2g-1)+\sqrt{1-4g}}{2ga^2/R^2-(2g-1)-\sqrt{1-4g}}\right| - \ln\left|\dfrac{1+\sqrt{1-4g}}{1-\sqrt{1-4g}}\right|\right) + F_2 \ln\dfrac{r}{a}, & \textit{when } g < 0.25. \end{cases} \tag{23}$$

According to the continuity condition of the elastic zone and plastic zones, that is, $\sigma_R^e = \sigma_R^p$, the radius R of the plastic zone can be obtained by numerical calculation.

3.5. Interaction between Roadway Surrounding Rock and Roadway Support. After the roadway is excavated, due to the stress release of surrounding rocks and the effect of

groundwater, the displacement of the tunnel wall is released, leading to a new stress equilibrium [36, 37]. After adding support to the surrounding rocks, the groundwater, surrounding rocks, and lining interact with each other again. To reflect this interaction, lining is regarded as a thick-walled cylinder under a uniform external pressure p_a. According to the Lame equation [35, 38, 39], the following is obtained:

$$p_a = \frac{E\prime}{a(1+u\prime)} \frac{a^2 - r_0^2}{(1-2u\prime)a^2 + r_0^2} (\overline{u}_a - \Delta u). \quad (24)$$

Here, r_0 is the inner radius, a is the outer radius, $E^{'}$ is the elastic constant of the surrounding rock material, u' is the elastic constant of the lining material, $\overline{u}_a$ represents the total displacement of the external tunnel wall after adding support, and Δu is the displacement of surrounding rocks released before adding support.

4. Example Verification and Discussions

This study uses geological data about surrounding rocks of mined roadways and lining in Beishan Lead–Zinc Mine, Guangxi, as calculation parameters. The lithology is limestone. The groundwater level elevation in the study area is 300.87–414.66 m. The groundwater is abundant, and the annual variation range is relatively large, generally around 40 m. Frequent and large water level fluctuations result in high water pressure and negative pressure effect on mining roadways, the surrounding rock, and the main factor of cracking. Table 2 indicates the mechanical parameters involved in this example.

When constructing groundwater seepage prevention and drainage systems in mining roadways, the safety of the roadway is always the top priority. However, it is impossible to avoid groundwater seepage completely. Therefore, in order to compare the characteristic curves of surrounding rocks of roadways under different drainage conditions, this study considers the following two drainage conditions by referring to Beishan Lead–Zinc Mine data: $p_1 = 0$ (full drainage) and $p_1 = 1.0p_f$ (no drainage), where p_1 is the roadway water pressure and p_f is the full water pressure.

4.1. Factors Influencing Radius of Plastic Zone after Rock Burst.

(1) The mining depth of the roadway is 145 m, and the resistance under support is not considered. Under the two drainage conditions described above, the correlation curve between the groundwater pressure on surrounding rocks p_0 and the radius of the plastic zone R/a is shown in Figure 3.

As shown in Figure 3, as the groundwater pressure rises when there is no drainage (i.e., in the water saturation state), the radius of the plastic zone R increases and the bearing capacity of surrounding rocks decreases gradually. When the bearing capacity of the surrounding rocks is completely lost, the curve tends to decline; under drainage conditions, the curve for the radius of the plastic zone R rises before leveling off, and the bearing capacity of surrounding rocks increases before reaching a relatively stable value. The curves under the two working conditions show that the stress of surrounding rocks in the upper part of the roadway will be significantly affected during excavation when there is a large volume of groundwater and changes in groundwater depth are significant. When the volume of groundwater is large, the radius of the plastic zone R is significantly affected by changes in groundwater depth. When the critical depth is reached, the stress of surrounding rocks will decrease rapidly and remain unsteady, and a slight disturbance of the surrounding rocks will lead to water inrush.

(2) When the depth of groundwater in the upper part of the roadway is 30 m, there is no support in the roadway (i.e.$p_a = 0$). Thus, the major factors affecting the radius of the plastic zone R are the depth of groundwater in the roadway and the effective porosity of the surrounding rock. The relationship curves are shown in Figure 4.

According to Figure 4, the radius of the plastic zone R increases as the groundwater depth and effective porosity increase, and the influence of the effective porosity grows as the degree of water drainage increases. The pore characteristics of rocks are different from those of general loose media, and the runoff of water in rocks is mainly layer fissure flow; thus, the effective porosity coefficient is used to modify the curve of effective pore stress change [33, 39, 40].

4.2. Correlation between Roadway Support and Surrounding Rock. When the height of groundwater in the upper part of the roadway is 70 m and the radius of the excavated roadway is 4 m, the curve of surrounding rock deformation characteristics is drawn according to two different drainage conditions, as shown in Figure 5.

Figure 5 shows that the surrounding rock support stress decreases and the displacement gradually increases under the two conditions; the characteristic curves gradually approach the x-axis while moving rightward across the graph. However, when the water is drained in the roadway, the stress is higher than that under the nondrainage condition. Besides, the change in displacement is smaller than that under the nondrainage condition, indicating the stability of surrounding rocks under the nondrainage condition is relatively weak.

Next, the roadways under the two working conditions in Figure 5 are supported by two different linings. The thicknesses of the linings are 0.2 m and 0.4 m, respectively, and the lining material is C_{30} concrete. When the displacement of the supporting roadway wall is released, Δu = 3cm, the relation curve of the supporting characteristics is shown in Figure 6.

Figure 6 shows that when the volume of water drainage remains the same, as the thickness of the lining increases, the support stiffness and resistance increase, and the

Table 2: Mechanical parameters of surrounding rock in the roadway and calculated parameters of lining.

Name	Poisson's ratio μ	Elasticity modulus E (GPa)	Gravity γ (kN · m^{-3})	The peak strength σ_c (MPa)	Frictional angle φ (°)	Permeability ratio in elastic-plastic zone ρ	Pore water pressure coefficient
Limestone	0.361	25.62	23.72	0.397	31.5	10.54	0.321
Lining	0.252	30.0	25.0	–	–	0.55	–
Limestone	0.314	24.94	22.97	0.418	34.4	11.27	0.347
Lining	0.193	30.0	25.0	–	–	0.55	–
Limestone	0.324	26.17	21.83	0.536	37.3	12.45	0.418
Lining	0.317	30.0	25.0	–	–	0.55	–
Limestone	0.262	24.67	22.49	0.385	32.4	10.28	0.313
Lining	0.261	30.0	25.0	–	–	0.55	–
Limestone	0.321	24.89	22.88	0.423	34.6	11.32	0.351
Lining	0.293	30.0	25.0	–	–	0.55	–
Limestone	0.318	26.26	21.91	0.527	37.61	12.33	0.429
Lining	0.417	30.0	25.0	–	–	0.55	–

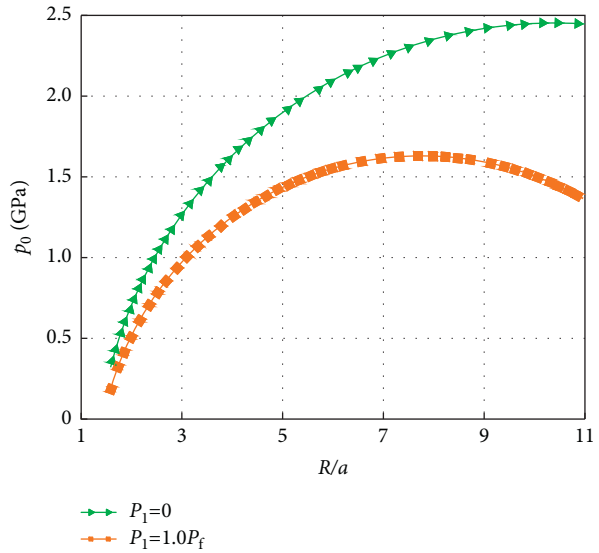

Figure 3: Correlation between groundwater pressure p_0 and R/a of the plastic region.

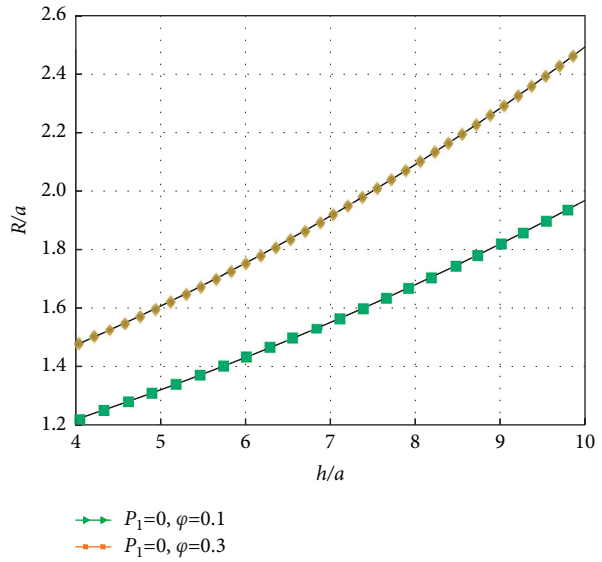

Figure 4: Relationship between R/a of plastic region and h/a under different water pressures and porosities. R/a is the size of the plastic expansion zone and h/a is the effective porosity water depth.

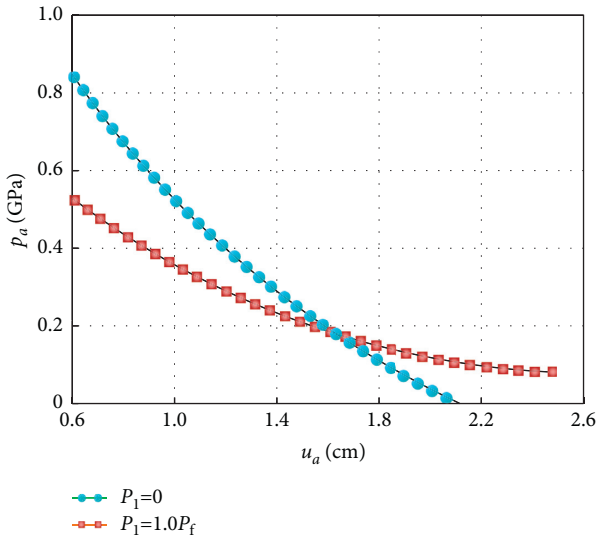

Figure 5: Characteristics of surrounding rock under different drainage conditions.

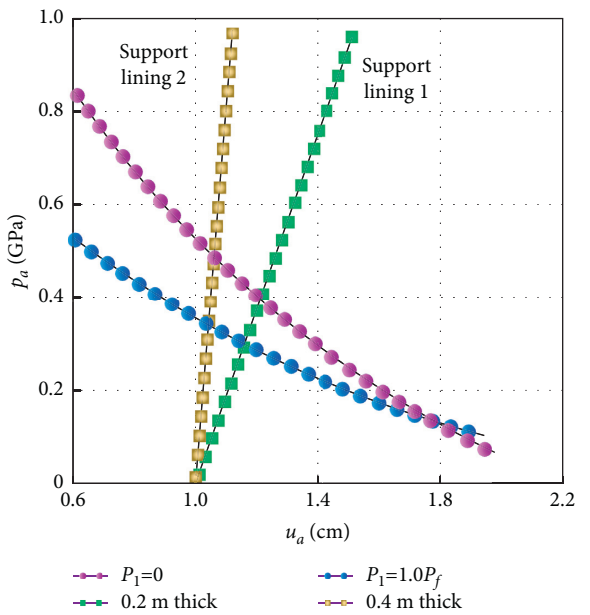

Figure 6: Comparison of surrounding rock characteristics before and after roadway support.

displacement of the roadway wall decreases. However, when the thickness of the lining continues to increase, the role of the supporting structure is not evident in further reducing the displacement of the roadway wall and improving the bearing capacity of surrounding rocks. Therefore, when adding support to mined roadways, it is necessary to determine the proper thickness of the lining, and the critical thickness should be determined according to the volume of groundwater drainage. When the critical thickness is balanced with the volume of groundwater drainage, an economical and reasonable lining thickness can be obtained.

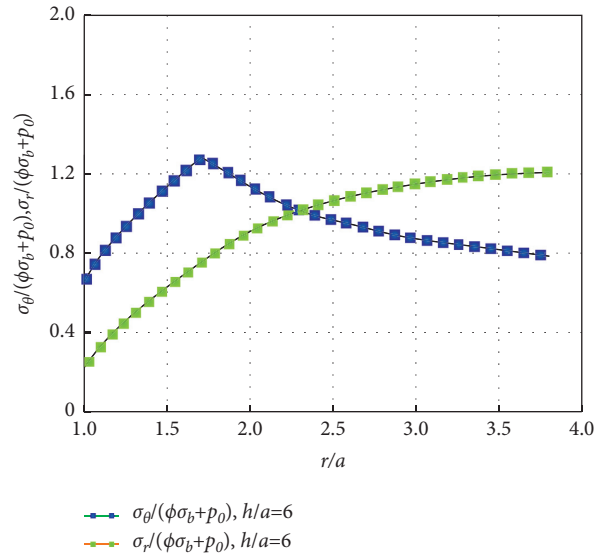

Figure 7: Stresses redistribution of surrounding rock after roadway excavation.

4.3. Law of Stress Distribution in Surrounding Rock. When the depth of groundwater in the upper part of the roadway is 30 m, $p_a = 0$, and $p_1 = 0$, the distribution of tangential stress and radial stress in the surrounding rock of the roadway after excavation presents a certain law of distribution, as described by the curves in Figure 7.

As Figure 7 shows, the ratio of original rock stress to radial stress presents different changing trends at the same point in the surrounding rock of the roadway under drainage and nondrainage conditions. Under the nondrainage condition, the tangential stress of surrounding rocks first increases and then decreases as the drainage volume grows. Under the drainage condition, the tangential stress increases gradually from the inner wall of the roadway to the outside and finally reaches a steady state. The two scenarios described above indicate that the peak stress of surrounding rocks decreases continuously in the expansion process of the plastic zone of surrounding rocks of roadways under the nondrainage condition; meanwhile, this peak stress increases continuously under the drainage condition.

4.4. Analysis and Determination of Minimum Support Resistance of Surrounding Rock. As shear slips continue to occur in the plastic zone in the roadway mining process, the surrounding rock begins to loosen and collapse to form a relaxation zone [39, 40], and the initial ground stress of the surrounding rock in the relaxation zone is higher than the normal tangential stress. The relation between the change in the loosening pressure and that in the deformation pressure of surrounding rocks can be reflected by the characteristic curve of surrounding rocks [41, 42]. The intersection point of the two curves is where the minimum surrounding rock pressure $p_{\min}$ is most likely to occur. It is essential to determine the value of $p_{\min}$ in support design. $p_{\min}$ can be

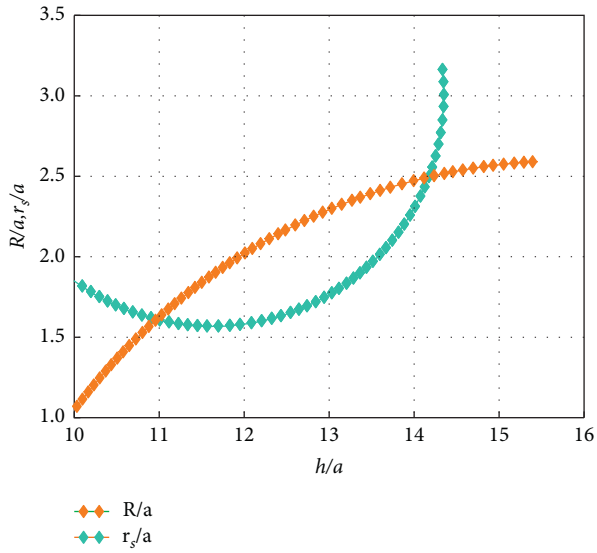

Figure 8: Relationship among h/a, R/a, and r_s/a.

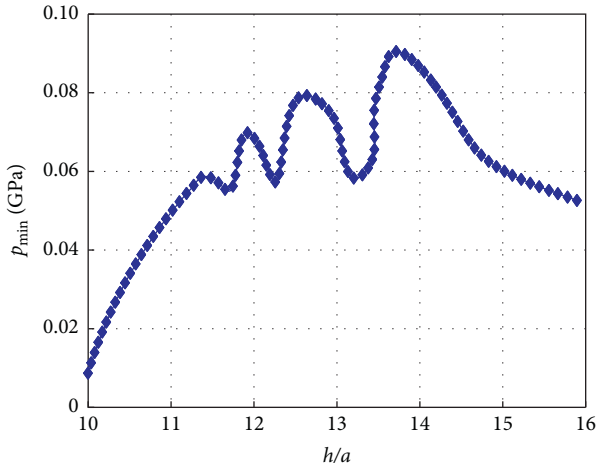

Figure 9: Relationship between $p_{\min}$ and h/a.

determined according to the equilibrium conditions in the relaxation zone established by Wang (2016) and Malkowski (2017):

$$p_{\min} = \gamma_{\text{sat}}(r_s - a), \tag{25}$$

where r_s is the radius of the relaxation zone.

Where $r = r_s$, the condition for continuity is $\sigma_\theta^p = \sigma_b + p_0$. Where $r = R$, the radial stress $\sigma_R^e = \sigma_R^p$ is the condition for continuity, and p_a in 20, (23), and (24) are replaced by $p_{\min}$ (in 25). Matlab can be used to solve for r_s and R. When the groundwater depth in the upper part of the roadway exceeds 30 m, the correlation among r_s, R, and $p_{\min}$ under different thicknesses of overlying strata is shown in Figures 8 and 9.

According to Figures 8 and 9, when the height of the groundwater head in the upper part of the roadway is higher than 30 m, the surrounding rock in the locally soft or fractured section appears in the relaxation zone, and the minimum support resistance of the lining decreases notably. In practice, when the support resistance reaches the minimum value $p_{\min}$, the surrounding rock will undergo ultimate deformation, the pressure of the surrounding rock after loosening is borne by the support structure, and the interaction between the surrounding rock and the support structure is deficient. This negatively influences the system's overall stability and is a significant cause for many high-pressure water mining accidents. Therefore, this kind of situation should be avoided.

5. Conclusions

(1) According to the numerical simulation method, the distribution law of stress and displacement of surrounding rock of roadways with deep and high-pressure water is studied. Considering the factors influencing the seepage of high-pressure water and different drainage conditions, we derived the analytical solution of the stress and displacement distribution of surrounding rock of the roadway under a complex stress state.

(2) During groundwater seepage, when the high-pressure head pressure of groundwater reaches the critical pressure for the stability of the surrounding rock of the roadway, the equilibrium state of the surrounding rock of the mined roadway is destroyed. At this time, surrounding rock easily loses stability and collapse may occur under slight disturbance, causing water inrush in the mine.

(3) The extent of plastic zone development is mainly affected by drainage conditions and effective porosity and increases with the increase in drainage and effective porosity. The supporting characteristic curve of fracturing range also changes with the increase in development of this zone. Therefore, in the design of waterproof linings and drainage systems during excavation of the tunnel, the seepage flow and the effective porosity should be determined after identifying the impacts of different drainage volumes so as to minimize their impact on the support structure and the stability of the surrounding rocks.

Data Availability

The test data used to support the findings of this study are included within the article.

Conflicts of Interest

No conflicts of interest exit in the submission of this manuscript.

Acknowledgments

This work was supported by Key R&D Plan Project of Guangxi Province of China (nos. AB18281013 and AB16380278), Natural Science Foundation of Guangxi Province of China (no. 2019GXNSFAA245011), and Special

Funds for Talents of Guangxi Province of China (no. 2016047).

References

[1] H. Jiang, D. Liu, W. Huang, Y. Xia, and F. Liu, "Creep properties of rock under high confining pressure and different pore water pressures and a modified Nishihara model," *Chinese Journal of Geotechnical Engineering*, vol. 36, no. 3, pp. 443–451, 2014.

[2] F. Wang, J. Xu, J. Xie, Z. Li, and J. Guo, "Mechanisms influencing the lateral roof roadway deformation by mining-induced fault population activation: a case study," *International Journal of Oil, Gas and Coal Technology*, vol. 11, no. 4, pp. 411–428, 2016.

[3] D. F. Zhu, S. H. Tu, H. S. Ma, and X. W. Zhang, "A 3D Voronoi and subdivision model for calibration of rock properties," *Modelling and Simulation in Materials Science and Engineering*, vol. 25, no. 8, p. 85, 2017.

[4] X. J. Li, H. M. Chen, Y. B. Sun, R. X. Zhou, and L. G. Wang, "Study on the splitting failure of the surrounding rock of underground caverns," *Geomechanics and Engineering*, vol. 14, no. 5, pp. 499–507, 2018.

[5] C. D. Sun, F. X. Jiang, Y. Liu, and Y. Y. Li, "Fractured zone of surrounding rock masses monitored by microseismic monitoring techniques in open backfilled mine using ultra high-water material," *Chinese Journal of Rock Mechanics and Engineering*, vol. 33, no. 3, pp. 475–483, 2014.

[6] Z. Huang, Z. Q. Jiang, Q. Sun, C. T. Ding, Y. J. Wang, and D. Zhang, "High-pressure water injection tests on permeability of deep rock mass under tunnels," *Chinese Journal of Geotechnical Engineering*, vol. 36, no. 8, pp. 1535–1543, 2014.

[7] S. Nasirimoghaddam, A. Mohebbi, M. Karimi, and M. R. Yarahmadi, "Assessment of pH-responsive nanoparticles performance on laboratory column flotation cell applying a real ore feed," *International Journal of Mining Science and Technology*, vol. 30, no. 2, pp. 197–205, 2020.

[8] J. Ning, J. Wang, Y. Tan, and Q. Xu, "Mechanical mechanism of overlying strata breaking and development of fractured zone during close-distance coal seam group mining," *International Journal of Mining Science and Technology*, vol. 30, no. 2, pp. 207–215, 2020.

[9] H. Bingxiang, Z. Xinglong, C. Shuliang, and L. Jiangwei, "Theory and technology of controlling hard roof with hydraulic fracturing in underground mining," *Chinese Journal of Rock Mechanics and Engineering*, vol. 36, no. 12, pp. 2954–2970, 2017.

[10] D. Zhu and S. Tu, "Mechanisms of support failure induced by repeated mining under gobs created by two-seam room mining and prevention measures," *Engineering Failure Analysis*, vol. 82, pp. 161–178, 2017a.

[11] A. Staniek, "Identification of grouting discontinuity of rock bolts as an efficient way to control safety conditions in mine roadways," *Journal of Mining World Express*, vol. 2, no. 1, pp. 9–22, 2013.

[12] J. Feifei, Z. Hui, L. Chang, and S. Jia, "Progress, prediction and prevention of rockbursts in underground metal mines," *Chinese Journal of Rock Mechanics and Engineering*, vol. 38, no. 5, pp. 956–972, 2019.

[13] Z. H. Zhao, X. J. Gao, Q. Ma, and S. J. Chen, "Impact hazard assessment of mine roadway excavation based on FAHP method," *Geotechnical & Geological Engineering*, vol. 37, no. 3, pp. 1859–1868, 2019.

[14] F. Wang, L. Shi, W. G. Fan, and C. Wang, "Application of computational geometry in coal mine Roadway3D localization," *The International Arab Journal of Information Technology*, vol. 15, no. 4, pp. 668–674, 2018.

[15] Y. Li, M. Lei, H. Wang et al., "Abutment pressure distribution for longwall face mining through abandoned roadways," *International Journal of Mining Science and Technology*, vol. 29, no. 1, pp. 59–64, 2019.

[16] Y. Zhang and L. Yang, "A novel dynamic predictive method of water inrush from coal floor based on gated recurrent unit model," *Natural Hazards*, vol. 105, no. 2, pp. 2027–2043, 2020.

[17] X. B. Zhang and M. Yang, "Determination of optimal extrication location of high extraction ro adway of large-mining-height fully mechanized face," *Advancesin Civil Engineering*, vol. 2018, Article ID 5145746, 7 pages, 2018.

[18] P. Pongpanya, T. Sasaoka, H. Shimada, A. Hamanaka, and S. Wahyudi, "Numerical study on effect of longwall mining on stability of main roadway under weak ground conditions in Indonesia," *Journal of Geological Resource and Engineering*, vol. 5, no. 3, pp. 93–104, 2017.

[19] F. Wang, C. Duan, S. Tu, N. Liang, and Q. Bai, "Hydraulic support crushed mechanism for the shallow seam mining face under the roadway pillars of room mining goaf," *International Journal of Mining Science and Technology*, vol. 27, no. 5, pp. 853–860, 2017.

[20] F. S. Han, X. L. Wu, X. Li, and D. K. Zhu, "Numerical simulation of phenomenon on zonal disintegration in deep underground mining in case of unsupported roadway," in *Proceedings of the IOP Conference Series: Earth and Environmental Science*, pp. 12–84, West Java, Indonesia, November 2018.

[21] Z. Cao, P. Xu, Z. Li, M. Zhang, Y. Zhao, and W. Shen, "Joint bearing mechanism of coal pillar and backfilling body in roadway backfilling mining technology(Article)," *Computers, Materials & Continua*, vol. 54, no. 2, pp. 137–159, 2018.

[22] P. O. T. Malkowski, L. K. S. Ostrowski, and P. O. T. Bachanek, "Modeling the small throw fault effect on the stability of a mining roadway and its verification by in situ investigation," *Energies*, vol. 10, no. 12, pp. 1996–1073, 2017.

[23] Z. Y. Wang, L. M. Dou, and G. F. Wang, "Mechanism analysis of roadway rockbursts induced by DynamicMining loading and its application," *Energies*, vol. 11, no. 9, pp. 1996–1073, 2018.

[24] H. P. Song, J. Q. Liu, F. B. Xue, and F. Q. Cheng, "Study of inorganic powders used for preparation of waterproof coating to coal mine roadways," *Polimery*, vol. 61, no. 11, pp. 844–849, 2016.

[25] P. Malkowski and Z. Niedbalski, "A comprehensive geomechanical method for the assessment of rockburst hazards in underground mining," *International Journal of Mining Science and Technology*, vol. 30, no. 3, 2020.

[26] T. Zhao, S. Yang, X. Hu, W. Song, J. Cai, and Q. Xu, "Restraining effect of nitrogen on coal oxidation in different stages:Non-isothermal TG-DSC and EPR research," *International Journal of Mining Science and Technology*, vol. 30, no. 3, 2020.

[27] H. Zhao, J. Li, Y. Liu, Y. Wang, T. Wang, and H. Cheng, "Experimental and measured research on three-dimensional deformation law of gas drainage borehole in coal seam," *International Journal of Mining Science and Technology*, vol. 30, no. 3, 2020.

[28] S. Wasilewski, "Gas-dynamic phenomena caused by rock mass tremors and rock bursts," *International Journal of Mining Science and Technology*, vol. 30, no. 3, 2020.

[29] J. Park and K. Kim, "Use of drilling performance to improve rock-breakage efficiencies: a part of mine-to-mill optimization studies in a hard-rock mine," *International Journal of Mining Science and Technology*, vol. 30, no. 2, pp. 179–188, 2020.

[30] A. Fleck, C. Couture, and V. Cabelguen, "Parallel personal measurements of diesel engine exhaust and crystalline silica using dual sampling port," *International Journal of Mining Science and Technology*, vol. 30, no. 3, pp. 313–319, 2020.

[31] H. Rehman, A. M. Naji, W. Ali, M. Junaid, R. A. Abdullah, and H. K. Yoo, "Numerical evaluation of new Austrian tunneling method excavation sequences: a case study," *International Journal of Mining Science and Technology*, vol. 30, no. 3, pp. 381–386, 2020.

[32] M. Åstrand, E. Jakobsson, M. Lindfors, and J. Svensson, "A system for underground road condition monitoring," *International Journal of Mining Science and Technology*, vol. 30, no. 3, pp. 405–411, 2020.

[33] H. Zhang, M. Tu, H. Cheng, and Y. Tang, "Breaking mechanism and control technology of sandstone straight roof in thin bedrock stope," *International Journal of Mining Science and Technology*, vol. 30, no. 2, pp. 259–263, 2020.

[34] E. Kabwe, "Confining stress effect on the elastoplastic ground reaction considering the Lode angle dependence," *International Journal of Mining Science and Technology*, vol. 30, no. 3, pp. 431–440, 2020.

[35] A. McQuillan, I. Canbulat, and J. Oh, "Methods applied in Australian industry to evaluate coal mine slope stability," *International Journal of Mining Science and Technology*, vol. 30, no. 2, pp. 151–155, 2020.

[36] A. Malinowska, R. Hejmanowski, and H. Dai, "Ground movements modeling applying adjusted influence function," *International Journal of Mining Science and Technology*, vol. 30, no. 2, pp. 243–249, 2020.

[37] V. Sobolev, N. Bilan, R. Dychkovskyi, E. C. Cabana, and A. Smolinski, "Reasons for breaking of chemical bonds of gas molecules during movement of explosion products in cracks formed in rock mass," *International Journal of Mining Science and Technology*, vol. 30, no. 2, pp. 265–269, 2020.

[38] Y. Zong, L. Han, Q. Meng, and Y. Wang, "Strength properties and evolution laws of cracked sandstone samples in re-loading tests," *International Journal of Mining Science and Technology*, vol. 30, no. 2, pp. 251–258, 2020.

[39] Y. Zhang, Y. Xie, Y. Zhang, J. Qiu, and S. Wu, "The adoption of deep neural network (DNN) to the prediction of soil liquefaction based on shear wave velocity," *Bulletin of Engineering Geology and the Environment*, vol. 80, no. 6, pp. 5053–5060, 2021.

[40] P. C. Pinazzi, A. J. S. Spearing, K. V. Jessu, P. Singh, and R. Hawker, "Mechanical performance of rock bolts under combined load conditions," *International Journal of Mining Science and Technology*, vol. 30, no. 2, pp. 167–177, 2020.

[41] Z. Tao, S. Yu, X. Yang, Y. Peng, Q. Chen, and H. Zhang, "Physical model test study on shear strength characteristics of slope sliding surface in Nanfen open-pit mine," *International Journal of Mining Science and Technology*, vol. 30, no. 33, pp. 421–429, 2020.

[42] Y. Zhou, D. Zhao, B. Li, H. Wang, Q. Tang, and Z. Zhang, "Fatigue damage mechanism and deformation behaviour of granite under ultrahigh-frequency cyclic loading conditions," *Rock Mechanics and Rock Engineering*, vol. 54, 2021.